Observations of Thermally-Driven Liquid Redistribution in a Partially Saturated Porous Medium

R. D. Manteufel and R. T. Green
Center for Nuclear Waste Regulatory Analyses
Southwest Research Institute
6220 Culebra Road
San Antonio, TX 78238-5166
(210)-522-5250 (phone)
(210)-522-5184 (fax)

ABSTRACT

Two laboratory experiments have been performed to investigate thermally-driven liquid redistribution in a partially saturated porous medium. The experiments consist of a sealed rectangular enclosure which was packed with unconsolidated medium (glass beads or alumina powders), and subjected to a steady-state temperature profile horizontally across the largest dimension of the enclosure. Experimental parameters were measured with a gamma-ray densitometer, tensiometers, thermistors, and visual observation aided with periodically-injected dye. The liquid was observed to vaporize near the hot wall, thereby creating a dry zone. The water vapor flowed to cooler regions of the medium where it condensed, thereby increasing the local saturation. Liquid was observed to be advected from the cooler regions towards the hot boundary. In the first experiment, an unanticipated observation was that a wet band (region of increased liquid saturation) developed on the cool side of the dryout zone, and that liquid was advected into the wet band. Based on initial experimental results, a second experiment with a different porous medium was conducted to reproduce the development of a wet band and associated dryout zone, and assess the important driving mechanisms for the observed liquid flow. Although less pronounced, liquid advection into the wet band was also observed in the second experiment.

NOMENCLATURE

D	=	effective porous medium diffusion coefficient (m^2/s)
D_C	=	capillary diffusivity (m^2/s)
$D_{WA,G}$	=	diffusion coefficient of water vapor in air (m^2/s)
g	=	gravitational constant ($9.81 m/s^2$)
h_{LG}	=	enthalpy of vaporization (J/kg)
I	=	counts in 60 s time period

I_d	=	counts in 60 s time period for dry medium ($S_L = 0$)
J	=	J-function (dimensionless)
$\vec{j}_{W,G}$	=	diffusive flux of water vapor in the gas [kg/(m^2-s)]
k_{SAT}	=	saturated permeability (m^2)
$k_{REL,L}$	=	relative liquid permeability (dimensionless)
M_W	=	molecular weight of water (18.02 kg/kgmole)
P	=	total gas pressure (N/m^2)
P_V	=	vapor pressure of water (N/m^2)
$P_{W,G}$	=	partial pressure of water vapor in the gas (N/m^2)
$P_{CAP/ADS}$	=	capillary/adsorptive pressure (N/m^2)
R	=	ideal gas constant [8314 J/(kgmole-K)]
R_{VP}	=	relative humidity (dimensionless)
S_L	=	liquid saturation (m^3 liquid/m^3 void)
t	=	time (s)
t_C	=	capillary time scale (s)
T	=	temperature (C)
T_O	=	reference temperature (C)
$\vec{v}_L$	=	liquid (Darcy) velocity (m/s)
α	=	van Genuchten parameters (1/m)
β	=	van Genuchten parameters (dimensionless)
η	=	advective enhancement factor (dimensionless)
σ	=	surface tension (N/m)
σ_O	=	reference surface tension (N/m)
ρ_L	=	liquid density (kg/m^3)
$\rho_{W,G}$	=	density of water vapor in the gas (kg/m^3)
ϕ	=	porosity (m^3 void/ m^3 medium)
μ_L	=	liquid viscosity [kg/(m-s)]
μ_w	=	linear attenuation coefficient for liquid water (1/cm)
τ	=	tortuosity (dimensionless)

INTRODUCTION

An understanding of thermally-driven fluid flow is needed to predict the performance of the proposed high-level nuclear waste repository. In particular, it is widely recognized that thermal processes (i.e., temperature and heat flux fields) and hydrologic processes (i.e., presence and flows of liquid water, water vapor and air) will significantly affect the processes and rates of: (i) waste container corrosion; (ii) waste form dissolution and mobilization; and (iii) radionuclide migration through the geologic medium. In addition, the U.S. Nuclear Regulatory Commission (NRC) has specified that

the thermal effects need to be considered in the assessment of the design of the repository (especially the stability of the mined excavations).

The emplacement of heat-dissipating nuclear waste is expected to vaporize the groundwater near the waste, thereby creating a dryout zone (Pollock, 1986; Pruess et al. 1990a,b; Buscheck and Nitao, 1992). The resulting water vapor is expected to flow into cooler regions of the medium where it will condense, thereby increasing the local saturation. A number of field experiments have been conducted (Patrick et al., 1986; Zimmerman et al., 1986; Rameriz et al., 1990) in order to study the effects of emplacing heat sources in partially saturated, fractured geologic media. In addition, laboratory experiments (Green et al., 1992; Manteufel et al., 1992) have been conducted to study the mechanisms of flow under well-controlled conditions. It is expected that both field and laboratory studies will be used to construct the knowledge base which will be used to predict and assess thermally-driven processes at the proposed repository.

The purpose of this paper is to present the setup and experimental results from two recent laboratory experiments. The experiments consisted of sealed rectangular enclosures which were packed with partially saturated, unconsolidated media. The two experiments were designed to be similar, yet with sufficient difference which would resolve hypotheses developed during the interpretation of the first experiment's results (herein called test 1). In particular, the second experiment (herein call test 2) differed from test 1 by: (i) additional tensiometers; (ii) additional thermistors; and (iii) different medium. Alumina powder was used in test 2 where glass beads were used in test 1. The media was changed in order to eliminate the potential thermal-chemical couplings observed in test 1. The primary purpose of performing test 2 was to investigate the development of a wet band in front of the dryout zone, and assess the existence and/or importance of hysteresis in the medium characteristic curves as a potential driving mechanism for liquid redistribution.

EXPERIMENTAL APPARATUS

The laboratory experiments consisted of a sealed rectangular enclosure (20.3 $\times$ 15.2 $\times$ 5.3 cm) with a clear plexiglass front wall (see Figure 1 for test 1, and Figure 2 for test 2). Each setup was instrumented with heat exchangers located on opposing sides across the longest dimension of the enclosure. The heat exchangers were connected to recirculating-fluid, constant-temperature baths which were used to maintain the side walls

at specified temperatures. As such, an approximately linear temperature profile was established horizontally throughout the medium. Experimental measurements were obtained using a gamma-ray densitometer, porous cup tensiometers, thermistors, and visual observation of periodically-injected dye. The locations of each of these measurements are shown in Figures 1 and 2.

Test 2 contained six tensiometers (whereas test 1 only had 2) which entered from the back of the apparatus and resided in the middle of the porous medium. In test 2, a thermistor was installed inside each of the tensiometers. Test 2 contained more thermistors than test 1, in order to assess both the horizontal and vertical temperature gradients. Gamma-ray densitometer measurements were taken at twenty-four locations (e.g., A1, A2, A3, ..., D6) throughout the duration of both tests. In test 2, horizontal gamma scans were taken at three levels designated as B, C and D. In both tests, two liquid-dye injection tubes entered from the back of the enclosure and extended to the front wall as shown in Figures 1 and 2.

The major differences between the setup of the two experiments were:

- glass beads were used in test 1, while alumina powder was used in test 2 as the unconsolidated porous medium
- the size distribution of glass beads used in test 1 was bi-modal with 50 percent by volume of factory-sieved beads from 28 to 53 μm, and 50 percent from 74 to 105 μm, and the alumina powder used in test 2 was factory sieved to particle sizes below 44 μm
- a simulated fracture was included in test 1, but not in test 2
- the right side heat exchanger temperature was controlled to be 60 C in the test 1 and 90 C in test 2
- the initial saturation was 65 percent in test 1, and 50 percent in test 2

Test 2 parameters were chosen to be different from test 1 for the following reasons:

- the test medium was changed to alumina powder to eliminate the potential for thermal-chemical effects due to the dissolution, mobilization, and precipitation of the glass that was observed in test 1

- a less well-sorted medium was used to establish a smoother characteristic curve (capillary pressure versus liquid saturation) to be more representative of unconsolidated porous media

- smaller sized particles were used to decrease the saturated permeability of the medium in order to accentuate the dryout zone,

- the temperature of the heated boundary was increased to 90 C to increase the thermal driving force for vaporization and vapor flow in order to accentuate the dryout zone

- the simulated fracture was eliminated because its effects (e.g., inhibiting liquid flow across the fracture) were not of interest in this study which focuses on the development of a wet band and associated dryout zone

EXPERIMENTAL RESULTS

Both tests were conducted for approximately 200 days which consisted of: (i) an ambient settling phase of 10-15 days; (ii) a heating phase of 85-100 days; (iii) a second ambient settling phase of 15-20 days; (iv) a drying phase of 15-20 days; and (iv) a saturating phase of 15-20 days. The initial ambient settling phase allowed the liquid water to redistribute under the influence of gravity, and was also used to setup and test instrumentation. In order to achieve an approximately-uniform initial saturation distribution, the water and medium were mixed prior to packing in the enclosure. During the heating period, the heat exchangers were maintained at the desired temperatures (20 C and 60 C for test 1, and 20 C and 90 C for test 2). A second ambient cooling period followed the heating period. The medium in test 2 was then dried by heating both heat exchangers to 90 C and passing dry nitrogen gas through the medium. The flow rate of nitrogen was controlled at a low rate so that the solid medium would not be disturbed and/or redistributed. The final phase of the tests consisted of introducing liquid water into the bottom of the enclosure at a sufficiently low rate in order to saturate the medium without disturbing the medium. Gamma-ray densitometer measurements were taken

during the drying and saturating phases in order to calibrate gamma-ray measurements taken during the heating phases.

An approximately linear temperature profile was established horizontally across the largest dimension of the enclosure in each test, thereby creating the thermal driving force for vaporization, vapor flow, condensation, and liquid flow. As a result, the observations were primarily one-dimensional (1D) in the horizontal direction. Experimental parameters were measured with a gamma-ray densitometer, porous cup tensiometers, thermistors, and visual observation aided with periodically-injected dye. In both experiments, liquid was observed to vaporize near the hot side creating a dry zone, and condense in cooler regions thereby increasing the liquid saturation. In test 1, a thin near-vertical band of high saturation (called a wet band) was observed to develop on the cool side of the dryout zone, and liquid (containing dye) was observed to be advected from the cooler regions into this region of increased saturation. The presence of a wet band was deduced from: (i) visual observations of the contrast of the medium through the front plexiglass wall (where wetter regions appeared darker and dryer regions appeared lighter); and (ii) gamma-ray densitometer measurements indicating an increased attenuation (hence increased liquid saturation) at the wet band and decreased attenuation (hence decreased liquid saturation) at measurement locations near the hot wall (e.g., C6 and D6 in Figure 1). In addition, the tensiometer data indicated that the hot side developed higher capillary/adsorptive pressures ($P_{CAP/ADS}$)[1]. Following an interpretation of test 1 results (Manteufel et al., 1992), it was hypothesized that either thermal-chemical effects or hysteresis in the characteristic curves of the medium was responsible for the observed liquid flow from apparently lower to higher saturation values. As a result, test 2 was designed and executed in order to: (i) eliminate thermal-chemical effects; (ii) reproduce (if possible) the development of a wet band in front of the dryout zone; and (iii) assess the transport mechanisms.

---

[1] In the literature, $P_{CAP/ADS}$ is also called the capillary pressure, matric potential, and/or suction pressure, among other terms. The term capillary/adsorptive pressure is adopted here for two reasons: (i) it clearly identifies the mechanisms which hold the water in the medium to be capillary and/or adsorptive forces, and (ii) it clearly identifies the units of measure to be pressure which can be interpreted as energy per unit volume.

Visual Observation

In test 1, visual observations (without the aid of dye) indicated that a dry zone developed near the hot side, and a nearly-vertical wet band developed in front of the dry zone, as illustrated in Figure 3. The medium near the hot wall was visually observed to lighten and this was interpreted that the local liquid saturation was lower. The dry zone was observed to be larger near the bottom of the test and narrower at the top of the test. Just to the left (or cool side) of the dry zone, a near-vertical band was visually observed to be darker than the surrounding medium and this was interpreted that the local liquid saturation increased. The wet band appeared thinner (~0.5 cm) and lighter near the top, while wider (~1 cm) and darker near the bottom of the medium. Hence, based on visual observations (without the aid of dye), a dry zone and a near-vertical wet band were interpreted to have developed in test 1. In test 2, the anticipated dry zone was visually observed, but the anticipated wet band was not (however the horizontal gamma-densitiometer scans suggest a wet band of ~1 cm).

Visual information was also obtained by periodically injecting dye through the dye injection tubes (see Figures 1 and 2) and then photographing the dye as it moved with the liquid in the medium. The dye injection tubes entered from the back of the enclosure and extended through the medium so that the dye was injected near the front wall (within 2-4 mm of the front wall). Having the dye injected near the front wall helped minimize the amount of fluid injected (approximately 0.1 ml per injection) while maximize the amount of visible dye. The dye used in the experiment is commercially available red food coloring which has been found to be highly soluble in water and found not to interact with the solid. It is assumed that the dye did not affect the liquid flow, but only allowed the flow to be visualized.

Dye was injected into test 1 during the 63rd day of heating and was observed for approximately 7 days, see Figure 4. Ten photographs show the movement of the two dye injections where the dye on the left side (near the cold wall) spread due to diffusion and had a small downward bulk movement. The dye on the right side (near the hot wall) diffused also, but it displayed a distinguishable bulk movement to the right (into a region of high liquid saturation) and then downward (within the region of high saturation).

In test 2, dye was injected at the same locations as in test 1. In Figure 5, ten photographs show the movement of the two dye injections starting on approximately the 60th day of the test. The sequence of photographs span only 8 hours of time due to the faster liquid velocities observed in test 2 (the difference in liquid velocities is related to the capillary diffusivity and is discussed in the analyses section). Within minutes after injection, the dye on the right side was observed to be advected towards the hot wall. In comparison, the dye on the left side exhibited primarily diffusion, but also some bulk advection toward the hot side.

Thermistors

Temperatures were measured at 10 locations in test 2 (see Figure 2 for locations) and the results are plotted in Figure 6. On the sixth day, the cooler was activated (maintaining both heat exchangers at 20 C), and on day 12 the heater was activated (maintaining the right heat exchanger at 90 C). Within less than one 1 day, a steady-state temperature profile was established throughout the experiment, indicating the insensitivity of heat transfer to fluid flow. The only major excursion in temperature recorded in the experiment was due to an electrical power failure to the laboratory (on the ~33rd day). Temperature scans for test 2 are plotted for five horizontal locations in Figure 6. From thermistors installed inside the tensiometers, the vertical temperature gradient was assessed to be approximately 0.09 C/cm near the hot side, and approximately 0.026 C/cm near the cold side. In comparison, the horizontal temperature gradient was approximately 4.47 C/cm, hence the temperature profile is considered to be primarily horizontally oriented.

The horizontal temperature profiles for test 1 and 12 are compared in Figure 7. As previously noted, the hot side temperature was increased from 60 to 90 C from test 1 to 12. The horizontal temperature profile for both tests is approximately linear throughout the domain with the exception of a sharper temperature drop near the hot side wall.

Tensiometers

Tensiometer measurements are plotted in Figures 8 and 9 for tests 6 and 12, respectively. Throughout the tests, the tensiometers near the hot side experienced higher $P_{CAP/ADS}$ indicating dryout. In test 1, the hot side tensiometer dried out three times and was refilled with water each time. The general trend of increasing $P_{CAP/ADS}$ near the hot

side is, however, still evident in Figure 8. In test 2, the hot side tensiometers experienced much higher $P_{CAP/ADS}$ and dried out quickly. Despite attempts to refill the tensiometers, the three tensiometers on the hot side failed to yield meaningful results except that they experience high values of $P_{CAP/ADS}$. The cold side tensiometers yielded much better results where the center-left tensiometer didn't dryout during the test. A trend in test 2 is that the $P_{CAP/ADS}$ rapidly decreases on the cold side and rapidly increases on the hot side after the heater is turned on. If one assumes that $P_{CAP/ADS}$ is proportional to surface tension (σ), then changes in σ will result in changes in $P_{CAP/ADS}$. By increasing the temperature on the hot side, σ would decrease thereby creating a gradient in $P_{CAP/ADS}$ which would move liquid from the hot to the cold side (this is discussed later). The time scale for liquid redistribution due to temperature-dependent surface tension appears to be small so that the redistribution process occurred quickly (within the first day). It appears that the liquid redistributed by accumulating on the cold side, hence increasing the liquid saturation and decreasing $P_{CAP/ADS}$.

Gamma-ray Densitometer

A ^{137}Cs gamma-ray source was used to produce a collimated beam (2.5 mm diameter) which was aimed at locations indicated in Figures 1 and 2. A gamma-ray detector was aligned with the beam on the back side of the test enclosure. The location of the source and detector were controlled with an xy-positioner which allowed the gamma beam to be passed through different locations of the experiment. The number of detected gamma rays (within an energy window near 0.661 MeV) were counted during 60 second intervals, after which the source/detector were positioned at a new location and another measurement taken. The attenuation of the gamma-ray beam through the test medium was measured using the detector. The number of counts was then used to infer the local liquid saturation using the attenuation principle:

$$I = I_d \exp(-\mu_w \phi S_L) \tag{1}$$

where

I	=	counts in 60 s time period,
I_d	=	counts in 60 s time period for dry medium ($S_L = 0$),
μ_w	=	linear attenuation coefficient for liquid water (1/cm),
ϕ	=	porosity (m^3 void/m^3 medium), and
S_L	=	liquid saturation (m^3 liquid/m^3 void).

Equation 1 can be solved for the saturation. Typically, the initial saturation is known so that liquid saturation can be expressed as a function of the initial counts for the initial saturation (for example):

$$S_L = 0.65 + \frac{1}{\mu_w \phi} \ln\left(\frac{I_{0.65}}{I}\right) \quad (2)$$

where

$I_{0.65}$ = counts in 60 s time period for medium with $S_L = 0.65$.

In Figure 10, liquid saturation values inferred from gamma ray attenuation measurements are plotted for eight locations (A1, A6, B1, B6, C1, C6, D1, D6) in test 1. Four of the measurement locations are near the hot side and four are near the cold side. The cold side measurements indicate a gradual buildup of liquid saturation throughout the duration of the test. The hot side measurements at locations D6 and C6 indicate a buildup of saturation followed by a reduction in saturation. At D6, the saturation was observed to reach a maximum of 0.85-0.9 near the 70th day of the test, thereafter the saturation level decreased. This was interpreted to indicate that the wet band had passed through the location D6 before day 70. At C6, the saturation reached ~0.85 near the 85th day which indicated that the wet band had reached the location near the end of the heating period of that test. Measurements at locations A6 and B6 indicate the approach of a wet band. This interpretation is consistent with the visual observations show in Figure 3, where the dryout zone is noted to be wider near the bottom of test 1.

In Figure 11, the liquid saturation values are plotted at eight locations in test 2. The gamma-ray measurements at the fixed locations did not indicate the presence of a wet band, as compared to test 1 measurements illustrated in Figure 10. In contrast, test 2 measurements do not appear to have a vertical trend where measurements in each column (e.g., column 1 and 6) are similar regardless of the row (e.g., A or D). The differences between column measurements are much more pronounced between the hot and cold side (i.e., between column 1 and 6). Soon after increasing the temperature of the right boundary, the cold side measurements indicated a rapid increase in liquid saturation (from 0.5 to 0.58) which remained constant throughout the duration of the test. At the same time, the hot side measurements indicated a rapid decrease in liquid saturation (from 0.5 to 0.38) which also remained constant throughout the remainder of the test. After the heating phase, the liquid saturation values returned to the ambient condition of 0.5 liquid saturation.

Additional data consisting of horizontal gamma-ray scans were recorded in test 2 (horizontal scans were not recorded in test 1). Scans recorded during two periods of the test 2 are illustrated in Figure 12. The scans were performed midway through the heating phase (~60th day), and near the end of the cooling phase (~105th day). The horizontal scans were recorded at three elevations (levels B, C and D). The heated scans indicate a gradual decrease (from left to right) in liquid saturation over most of the medium, with a sharper decrease near the hot side. From these measurements, the dryout zone is noticeable near the hot side. There appears to be a slight buildup of saturation (ΔS_L ~ 0.05) near the dryout zone, indicating the presence of a wet band. This region of increased saturation was not visibly distinguishable from observations through the front plexiglass wall (where in test 1 it was distinguishable), hence the horizontal gamma-ray scans are the only data indicating this phenomenon. After the heating phase, the horizontal gamma scans indicate that the liquid redistributed throughout the medium to an ambient level of 0.5 liquid saturation. The only noticeable exception is near the hot side where the liquid saturation only partially recovered to the initial 0.5 saturation level.

ANALYSES

In Appendix A, a one-dimensional mathematical model is developed for the conservation of water in a nonisothermal, partially saturated ($S_L < 1.0$) porous medium which includes the liquid advection and vapor diffusion, and the final equation is repeated here:

$$\rho_L \phi \frac{\partial S_L}{\partial t} = \frac{\partial}{\partial x}\left(\frac{\rho_L k_{SAT} k_{REL,L}}{\mu_L}\left[\left(\frac{-d P_{CAP/ADS}}{d S_L}\right)\frac{\partial S_L}{\partial x} + \frac{P_{CAP/ADS}}{\sigma}\left(\frac{-d\sigma}{dT}\right)\frac{\partial T}{\partial x}\right]\right) + \frac{\partial}{\partial x}\left(\eta D \rho_{W,G}\left[\frac{h_{LG} M_W}{R T^2}\frac{\partial T}{\partial x} + \frac{M_W}{\rho_L R T}\left(\frac{-d P_{CAP/ADS}}{d S_L}\right)\frac{\partial S_L}{\partial x}\right]\right) \quad \text{(A-12)}$$

In Eq. A-12, the transfer mechanisms have been related to either saturation or temperature gradients which are useful because saturation typically is the independent variable of interest and temperature is typically a known quantity (or an experimentally controlled dependent variable). Three aspects of the theoretical model are discussed below: (i) capillary diffusivity; (ii) liquid redistribution due to temperature-dependent surface tension; and (iii) the vaporization/condensation source term for liquid water.

Capillary Diffusivity

The capillary diffusivity can be identified in Eq. A-12 to be (which is consistent with the literature):

$$D_C = \frac{k_{SAT} k_{REL,L}}{\phi \mu_L} \left(\frac{-d P_{CAP/ADS}}{d S_L} \right) \tag{3}$$

The diffusivity can be used to indicate how quickly the liquid saturation will respond to changes in the system (such as changes in saturation at the boundary). For test 2, the capillary diffusivity was estimated to be $D_C \sim 10^{-6}$ m^2/s (near $S_L = 0.5$ and decrease slightly with decreasing S_L) while for test 1 it was estimated to be at least one decade smaller.

The capillary time scale for liquid advection is given by the familiar equation:

$$t_C \sim \frac{L^2}{D_C} \tag{4}$$

For test 2, the capillary time scale was estimated to be $t_C \sim 6$ hours while for test 1 it was $t_C \sim 60$ hours (2.5 days). The difference in D_C is due primarily to differences in $dP_{CAP/ADS}/dS_L$. The permeability for test 1 was assessed to be comparable to that of test 2 which was $k_{SAT} \sim 10^{-15}$ m^2. The derivative of capillary/adsorptive pressure with respect to liquid saturation can be estimated from Figure 13 to be $dP_{CAP/ADS}/dS_L \sim 5 \times 10^5$ Pa per 100 percent saturation for test 2 and $dP_{CAP/ADS}/dS_L \sim 2 \times 10^4$ Pa per 100 percent saturation for test 1. This simple analysis helps explain the experimental observation that test 2 responded faster to changes than test 1. By comparison of Figures 4 and 5, the dye in test 1 was tracked from time of the injection for ~ 7 days while in test 2 it was tracked for ~1/3 day (which is approximately one order of magnitude smaller). Hence the capillary diffusivity and the capillary time scale have been identified in the mathematical model and assessed to be in qualitative agreement with the observation that test 2 responded faster than test 1.

Liquid Redistribution due to Temperature-Dependent Surface Tension

One observation in test 2 was that liquid quickly redistributed (within ~1 day) after the heater was turned on thereby increasing the saturation on the cool side and

decreasing the saturation on the hot side. One possible mechanisms for this redistribution is that temperature-dependent surface tension pulled liquid from the hot side toward the cool side because surface tension decreases with increasing temperature. At equilibrium (neglecting the influence of vaporization/condensation) the temperature gradient induces a gradient in $P_{CAP/ADS}$ which is balanced by a saturation gradient (from Eq. A-12):

$$\left(\frac{-d\,P_{CAP/ADS}}{d\,S_L}\right)\frac{\partial\,S_L}{\partial\,x} = -\frac{P_{CAP/ADS}}{\sigma}\left(\frac{-d\,\sigma}{d\,T}\right)\frac{\partial\,T}{\partial\,x} \tag{5}$$

Because the temperature gradient is linear, Eq. 5 can be expressed as:

$$\Delta S_L \equiv -\frac{\frac{1}{\sigma}\left(\frac{-d\,\sigma}{d\,T}\right)}{\frac{1}{P_{CAP/ADS}}\left(\frac{-d\,P_{CAP/ADS}}{d\,T}\right)}\Delta T \tag{6}$$

With $\sigma \sim 0.073$ N/m, and $d\sigma/dT \sim -0.00017$ N/(m-C), the imposed temperature gradient in test 2 ($\Delta T \sim 70$ C) leads to an assessment that the maximum change in saturation from hot to cool side would be $\Delta S_L \sim 0.07$ which is less than the experimentally observed value of $\Delta S_L \sim 0.2$. Nevertheless, the direction and approximate magnitude of the liquid redistribution predicted by the theoretical model (due only to temperature-dependent surface tension) is in qualitative agreement with the experimental observations.

Condensation/Vaporization Source Term for Liquid Water

The second term on the right hand side of Eq. A-12 represents a source/sink term of liquid water due to vapor flow with condensation/vaporization. When a medium is subjected to a temperature gradient, liquid will vaporize in the regions of higher temperature (which represents a sink for liquid water) and condense in regions of lower temperature (which represents a source for liquid water). The distribution of vaporization/condensation can be assessed where two groups of terms are present in the second right hand side of Eq. A-12 due to the dependence on temperature (through the vapor pressure and Claperyon equation) and dependence on saturation (through the capillary/adsorptive pressure and Kelvin equation). The temperature gradient is considered the primary driving mechanisms for vapor flow, and the gradient in saturation becomes important only as $P_{CAP/ADS}$ becomes large (i.e., the medium becomes dry). In a dry medium the relative humidity can be less than 100 percent due to vapor pressure lowering as predicted by the Kelvin equation (Eq. A-11). Outside the dryout zone, the condensation/vaporization source term can be approximated as:

$$Q_{V/C} \equiv \frac{\partial}{\partial x}\left(\eta D \frac{h_{LG}(M_W)^2 P_V}{R^2 T^3} \frac{\partial T}{\partial x}\right) \tag{7}$$

In Eq. 7, three terms are noted to be temperature dependent (hence spatially dependent): η, T^{-3}, and P_V. In Figure 14, the temperature dependence of the terms are compared where it can be noted that the P_V is the most temperature dependent term. Hence, the other terms can be considered approximately constant and removed outside the spatial derivative, leading to a simplified model for $Q_{V/C}$:

$$Q_{V/C} \equiv \frac{\eta D (h_{LG})^2 (M_W)^3 P_V}{R^3 T^5} \left(\frac{\partial T}{\partial x}\right)^2 \tag{8}$$

From Eq. 8, the condensation source term is proportional to the temperature gradient squared and proportional to the vapor pressure. Hence, in an experiment the importance of vaporization/condensation (i.e., vapor flow) can be increased by increasing the temperature gradient. The vapor pressure is strongly temperature dependent [i.e., $P_V \sim \exp(-1/T)$] as illustrated in Figure 14. Because $Q_{V/C} \sim P_V$, the source of liquid condensation is largest near the highest temperature (which is also near the source of vaporization) for a medium subject to a linear temperature gradient (such as in Tests 6 and 12). In comparison, the zone of vaporization is small and located at the point of maximum temperature. As time progresses, vaporization removes enough liquid to create a dryout zone (within which vapor pressure lowering may be important). With this model, the region of vaporization is predicted to be small and located near the region of maximum temperature, and the region of condensation will be much larger and strongest near the region of vaporization, as illustrated in Figure 15. Because the region of maximum condensation is located to the cool side of the vaporization, it will tend to locally increase the liquid saturation (i.e., create a wet band) which was observed in the tests. Hence the model predicts a distribution of $Q_{V/C}$ which accentuates the development of a wet band and is in qualitative agreement with the experimental observations.

CONCLUSIONS

A laboratory experimental study of thermally-driven liquid redistribution in partially saturated porous medium, has been conducted and reported herein. The experimental set-up consisted of a sealed rectangular enclosure subject to a steady-state

temperature profile across the largest enclosure dimension. The experimental results indicate that:

- vaporization, vapor flow, condensation, and liquid advection are important mass transfer mechanisms for water in a nonisothermal porous medium
- a relatively small dryout zone developed near the hot side in both tests
- the local liquid saturation increased throughout the majority of the porous volume of the experiment due to the displacement of liquid in the dryout zone
- the liquid saturation profile was predominately one-dimensional (due to the imposed temperature profile being predominately one-dimensional)
- the largest gradients in liquid saturation occurred near the dryout zone
- a wet band developed in front of the dryout zone and was more pronounced in test 1 which used glass beads (instead of alumina powder in test 2) for the porous medium and subjected to a smaller temperature gradient.

A simplified mathematical model has been developed and used to assess the capillary diffusivity, the temperature dependent surface tension, and condensation/vaporization source term. Conclusions from the theoretical analyses include:

- the capillary diffusivity and time scale have been identified and found to be in qualitative agreement with the experimental observation that test 2 responded more quickly than test 1
- a model for liquid redistribution due to temperature dependent surface tension has been developed and found to be in qualitative agreement with experimental observations
- a model for condensation/vaporization source term for liquid water has been developed and found to be in qualitative agreement with the experimental observation of the development of a wet band

ACKNOWLEDGMENTS

This report was prepared to document work performed by the Center for Nuclear Waste Regulatory Analyses (CNWRA) for the U.S. Nulcear Regulatory Commission under Contract No. NRC-02-88-005. The activities reported here were performed on behalf of the NRC Office of Nuclear Regulatory Research, Division of Regulatory Applications. The report is an independent product of the CNWRA and does not necessarily reflect the views or regulatory position of the NRC.

APPENDIX A

In this appendix, the one-dimensional mathematical model for the conservation of water in a nonisothermal, partially saturated medium:

$$\rho_L \phi \frac{\partial S_L}{\partial t} = -\frac{\partial}{\partial x}(\rho_L \vec{v}_L) - \frac{\partial}{\partial x}(\vec{j}_{W,G}) \qquad \text{(A-1)}$$

where the variables are defined in the list of nomenclature. In the model, the accumulation of water vapor is neglected (in comparison with the accumulation of liquid water) due to $(\rho_{W,G} / \rho_L) << 1$. The important mechanisms for water redistribution are (i) liquid phase advection ($\vec{v}_L$), (ii) gas phase (i.e., vapor) molecular diffusion ($\vec{j}_{W,G}$), and (iii) gas phase advection. The gas phase advection is included in the model for the molecular diffusion. The liquid advection is modeled using Darcy's Law:

$$\vec{v}_L = -\frac{k_{SAT} k_{REL,L}}{\mu_L} \frac{\partial}{\partial x}(-P_{CAP/ADS}) \qquad \text{(A-2)}$$

The capillary/adsorptive pressure can be modeled using the J-function (Leverett et al., 1942) times a constant scaling factor:

$$P_{CAP/ADS} = \frac{\sigma \rho_L g}{\sigma_O \alpha} J \qquad \text{(A-3)}$$

The J-function can be based on the van Genuchten model:

$$J = \left((S_L)^{(\beta/(1-\beta))} - 1\right)^{\frac{1}{\beta}} \qquad \text{(A-4)}$$

The molecular diffusion of water in the gas phase is based on a modified Fick's law to approximately account for advective gas flow induced by the diffusion of water vapor:

$$\vec{j}_{W,G} = -\eta D \frac{\partial}{\partial x}(\rho_{W,G}) \qquad \text{(A-5)}$$

The advective enhancement factor is:

$$\eta = \frac{P_G}{P_G - P_{W,G}} \tag{A-6}$$

and the effective porous medium diffusion coefficient is:

$$D = \tau \phi (1 - S_L) D_{WA,G} \tag{A-7}$$

The water vapor is assumed to behave as an ideal gas:

$$\rho_{W,G} = \frac{P_{W,G} M_W}{R T} \tag{A-8}$$

The partial pressure of water in the gas is related to the vapor pressure and the relative humidity (or reduction in vapor pressure):

$$P_{W,G} = P_V R_{VP} \tag{A-9}$$

The Claperyon equation can be used to express P_V as a function of temperature:

$$P_V = P_{VO} \exp\left(\frac{h_{LG} M_W}{R}\left(\frac{1}{T_O} - \frac{1}{T}\right)\right) \tag{A-10}$$

The Kelvin equation can be used to express R_{VP} as a function of $P_{CAP/ADS}$:

$$R_{VP} = \exp\left(\frac{-P_{CAP/ADS} M_W}{\rho_L R T}\right) \tag{A-11}$$

Equations A-2 through A-11 can be inserted into Eq. A-1 to yield:

$$\rho_L \phi \frac{\partial S_L}{\partial t} = \frac{\partial}{\partial x}\left(\frac{\rho_L k_{SAT} k_{REL,L}}{\mu_L}\left[\left(\frac{-d P_{CAP/ADS}}{d S_L}\right)\frac{\partial S_L}{\partial x} + \frac{P_{CAP/ADS}}{\sigma}\left(\frac{-d\sigma}{dT}\right)\frac{\partial T}{\partial x}\right]\right) + \frac{\partial}{\partial x}\left(\eta D \rho_{W,G}\left[\frac{h_{LG} M_W}{R T^2}\frac{\partial T}{\partial x} + \frac{M_W}{\rho_L R T}\left(\frac{-d P_{CAP/ADS}}{d S_L}\right)\frac{\partial S_L}{\partial x}\right]\right) \tag{A-12}$$

Equation A-12 is used in the analyses section of this paper.

REFERENCES

Buscheck, T.A. and J.J. Nitao. 1992. The impact of thermal loading on repository performance at Yucca Mountain. *Proceedings of the International High-Level Radioactive Waste Management Conference*. La Grange Park, IL: American Nuclear Society: 1003-1017.

Green, R.T., R.D. Manteufel, F.T. Dodge, and S.J. Svedeman. 1992. *Theoretical and Experimental Investigation of Thermohydrologic Processes in a Partially Saturated, Fractured Porous Medium.* NUREG/CR-6026, CNWRA 92-006. Washington, DC: Nuclear Regulatory Commission.

Manteufel, R.D., R.T. Green, F.T. Dodge, and S.J. Svedeman. 1992. An experimental investigation of two-phase, two-component, nonisothermal flow in a porous medium with a simulated fracture. I. Catton editor. *Heat and Mass Transfer in Porous Media.* HTD-216. New York: American Society of Mechanical Engineers: 9-18.

Nitao, J.J. 1991. *V-TOUGH—An Enhanced Version of the TOUGH Code for the Thermal and Hydrologic Simulation of Large-Scale Problems in Nuclear Waste Isolation.* UCID-21954. Livermore, CA: Lawrence Livermore National Laboratory.

Patrick W.C. et al. 1986. *Spent Fuel Test—Climax: An evaluation of the Technical Feasibility of Geologic Storage of Spent Nuclear Fuel in Granite.* UCRL-53702. Livermore, CA: Lawrence Livermore National Laboratory.

Pollock D.W. 1986. Simulation of fluid flow and energy transport processes associated with high-level radioactive waste disposal in unsaturated alluvium. *Water Resources Research* 22(5): 765-775.

Pruess K., J.S.Y. Wang, and Y.W. Tsang. 1990a. On thermohydrologic conditions near high-level nuclear wastes emplaced in partially saturated fractured tuff. 1. Simulation studies with explicit consideration of fracture effects. *Water Resources Research* 26(6): 1235-1248.

Pruess K., J.S.Y. Wang, and Y.W. Tsang. 1990b. On thermohydrologic conditions near high-level nuclear wastes emplaced in partially saturated fractured tuff. 2. Effective continuum approximation. *Water Resources Research* 26(6): 1249-1261.

Rameriz, A.L. (editor), T. Buscheck, R. Carlson, W. Daily, K. Lee, W. Lin, N. Mao, A. Ramirez, T. Ueng, H. Wang, and D. Watwood. 1991. *Prototype Engineered Barrier Systems Field Test (PEBSFT) Final Report.* UCID-106159. Livermore, CA: Lawrence Livermore National Laboratory.

van Genuchten, M.T. 1980. A closed-form equation for predicting the hydraulic conductivity of unsaturated soils. *Soil Science Society of America Journal* 44: 892-898.

Zimmerman, R.M., M.L. Blanford, J.F. Holland, R.L. Schuch, and W.H. Barrett. 1986. *Final Report: G-Tunnel Small-Diameter Experiments.* SAND84-2621. Albuquerque, NM: Sandia National Laboratories.

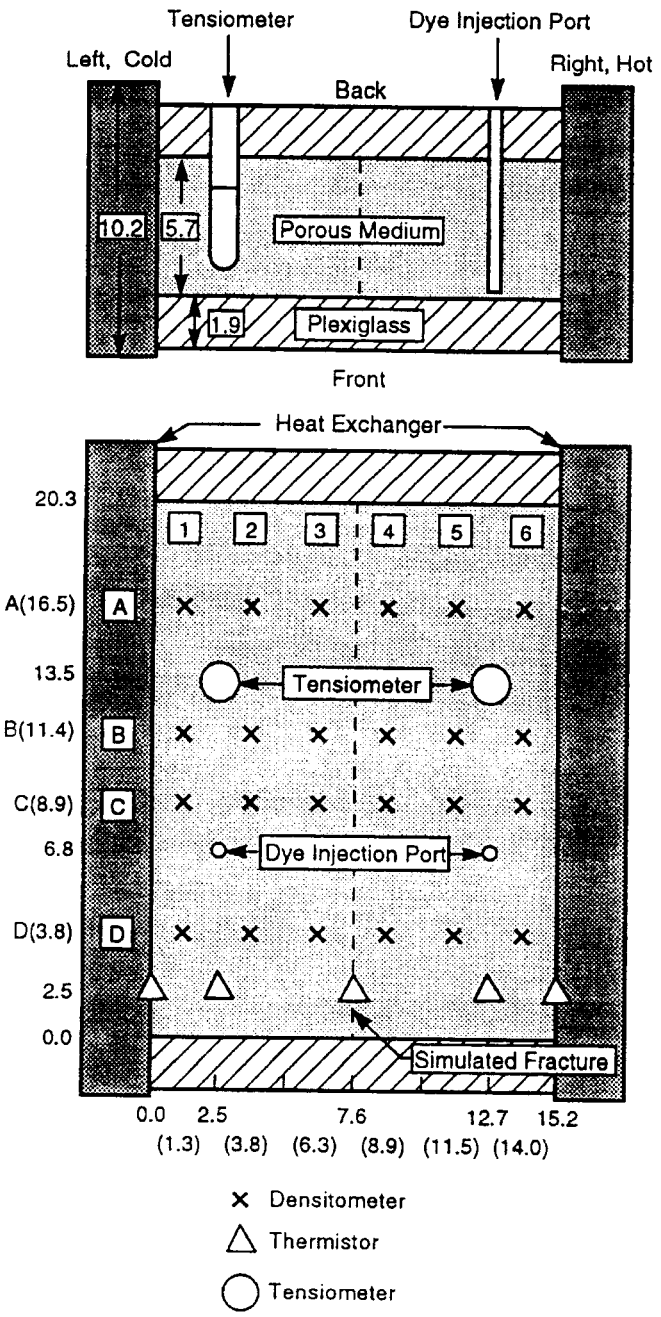

Figure 1. Test 1 experimental setup (all dimensions in cm).

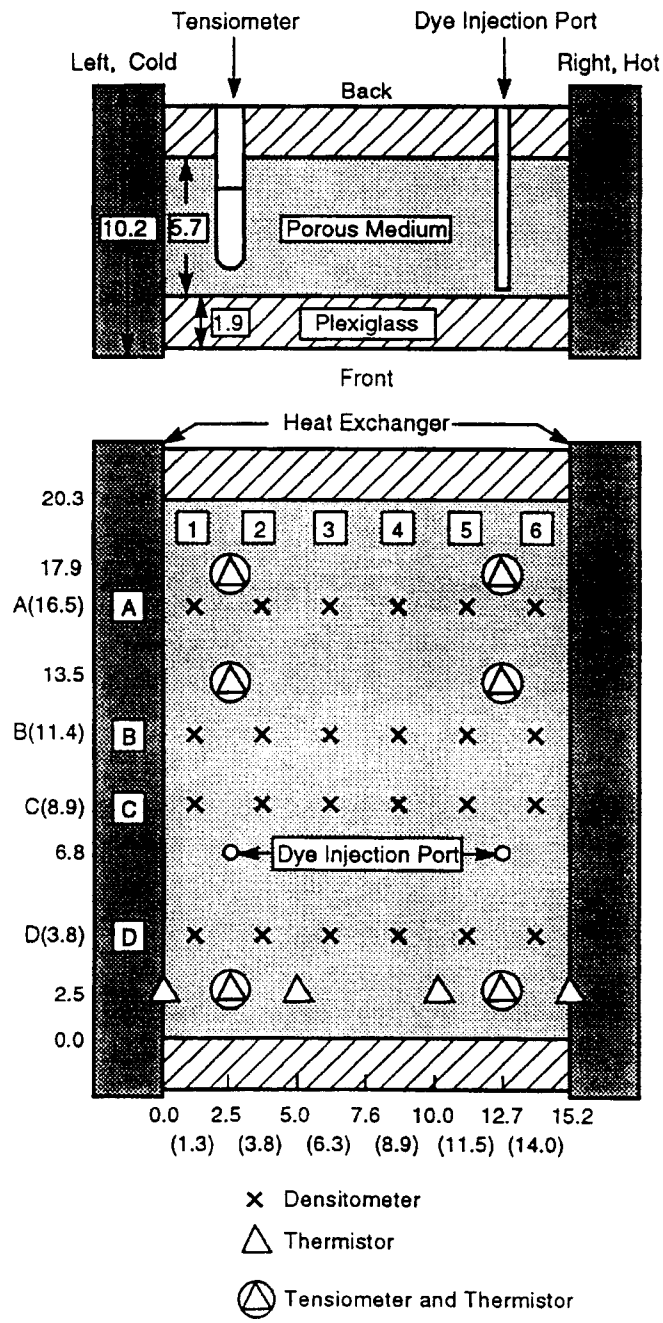

Figure 2. Test 2 experimental setup (all dimensions in cm).

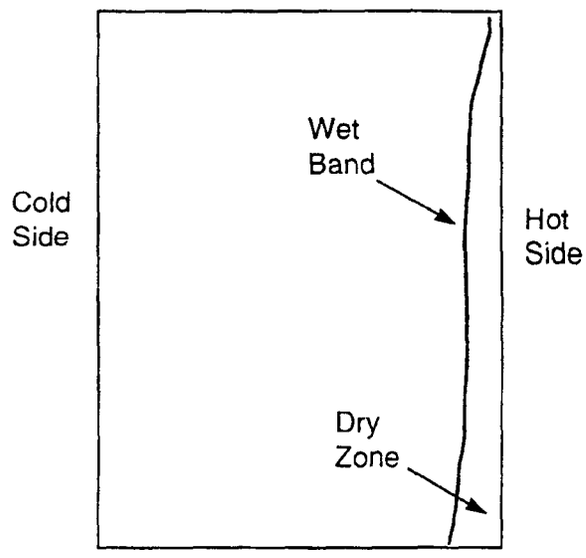

Figure 3. Location of the observed dry zone and wet band in test 1.

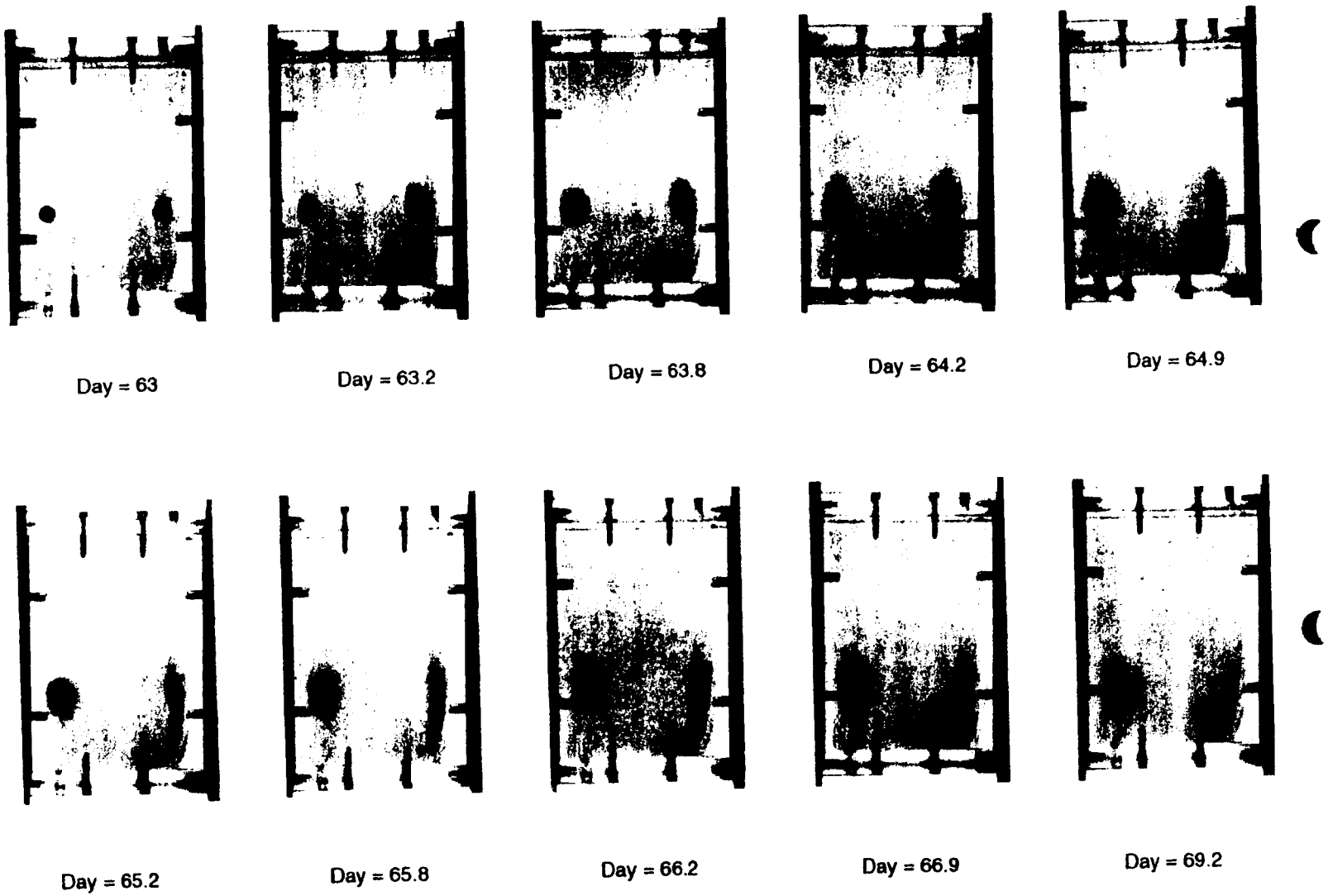

Figure 4. Ten photographs in test 1 showing dye locations after injection into the hot side port (right) and cold side port (left).

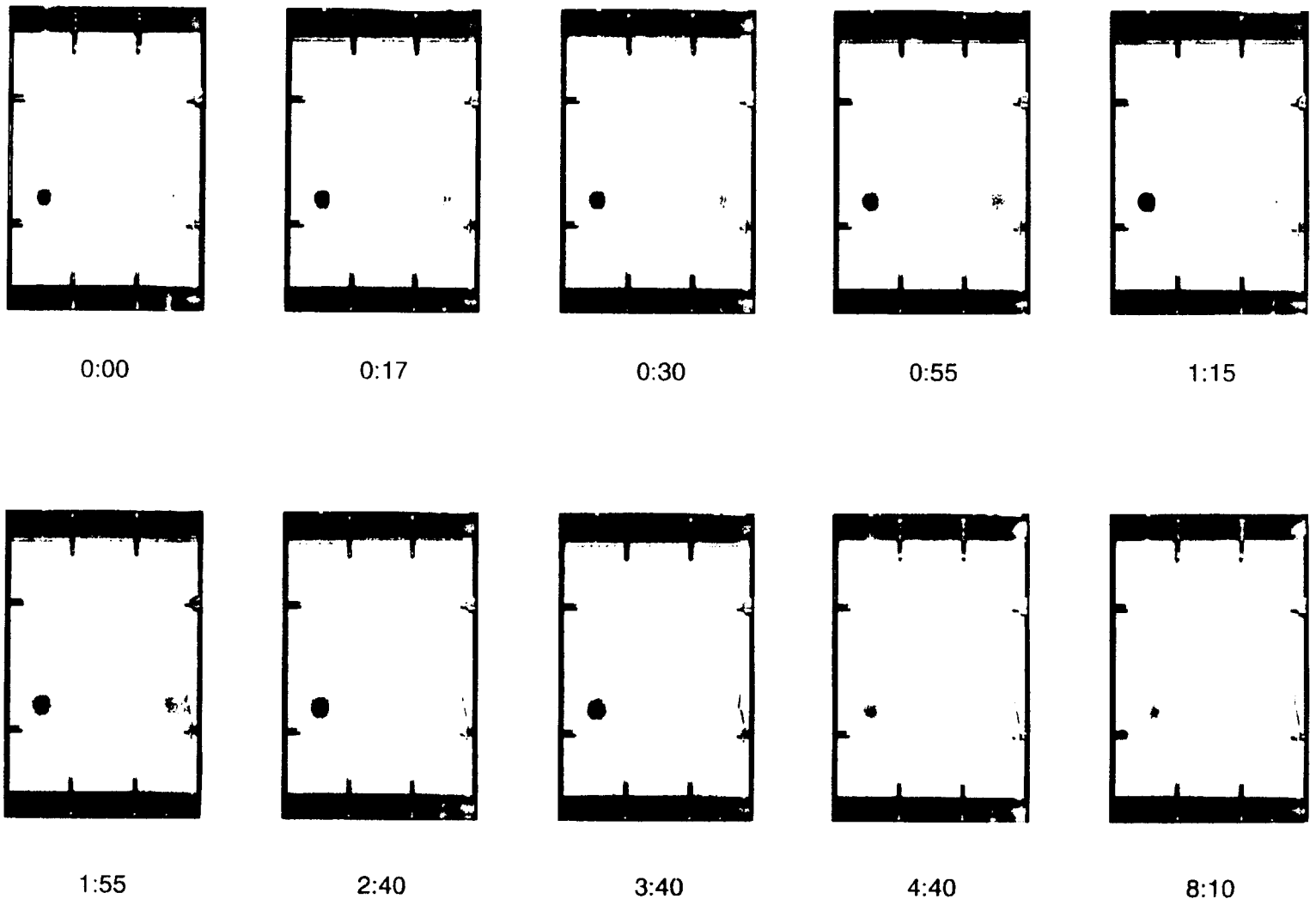

Figure 5. Ten photographs in test 2 showing dye locations after injection into the hot side port (right) and cold side port (left). Time measured in hours:minutes after injection.

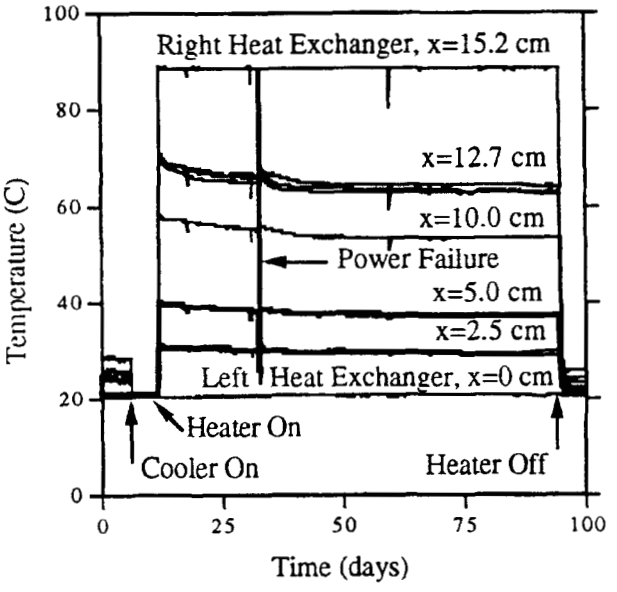

Figure 6. Temperature measurements in test 2.

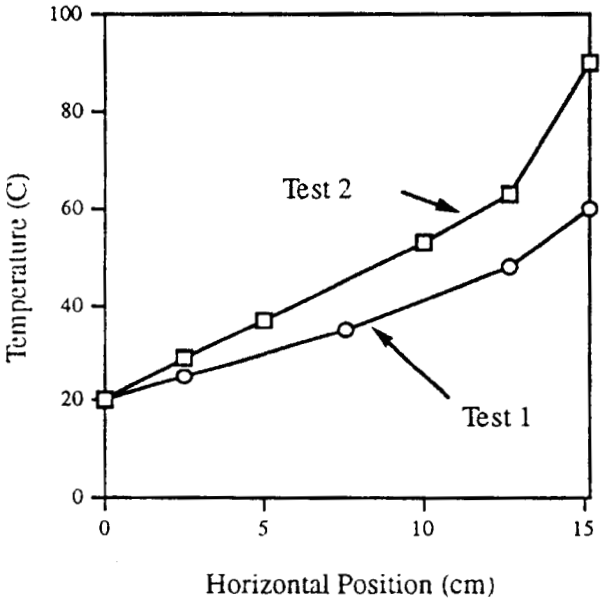

Figure 7. Steady-state, horizontal temperature profiles.

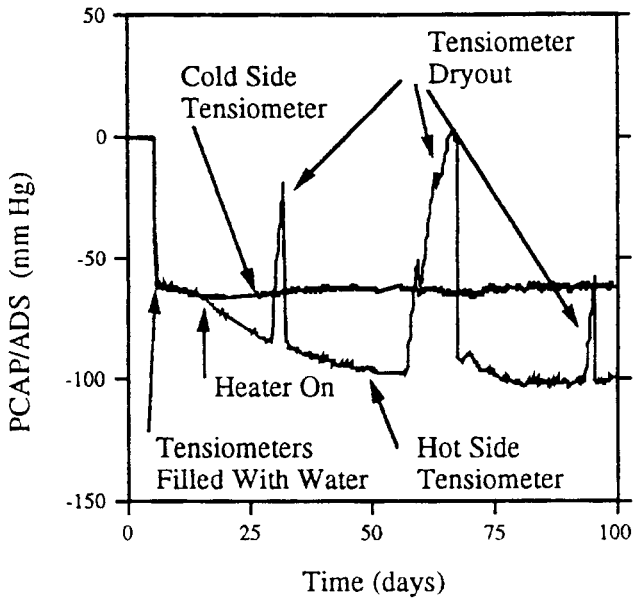

Figure 8. Tensiometer measurements in test 1.

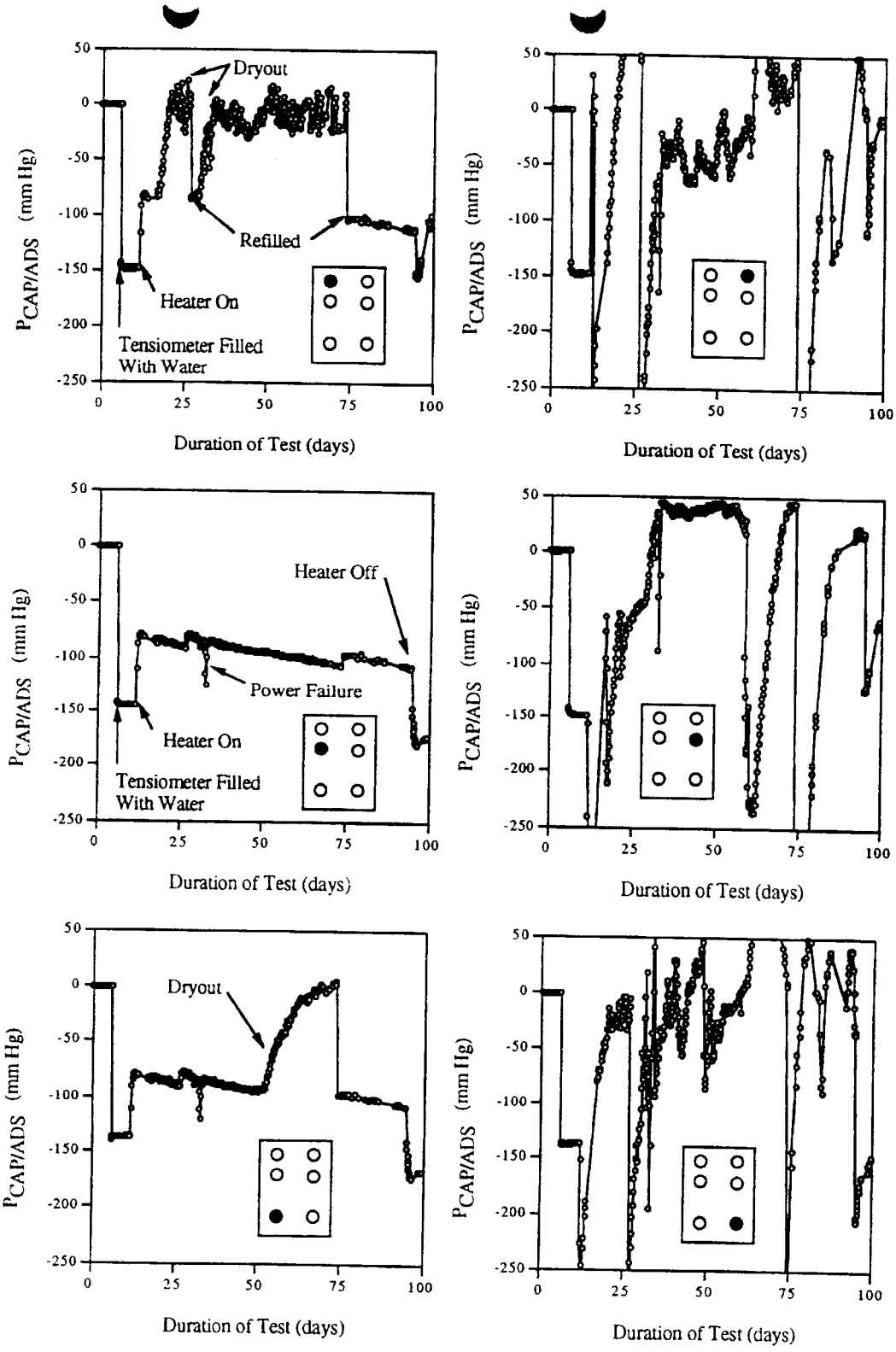

Figure 9. Tensiometer measurements in test 2 (insets show measurement locations).

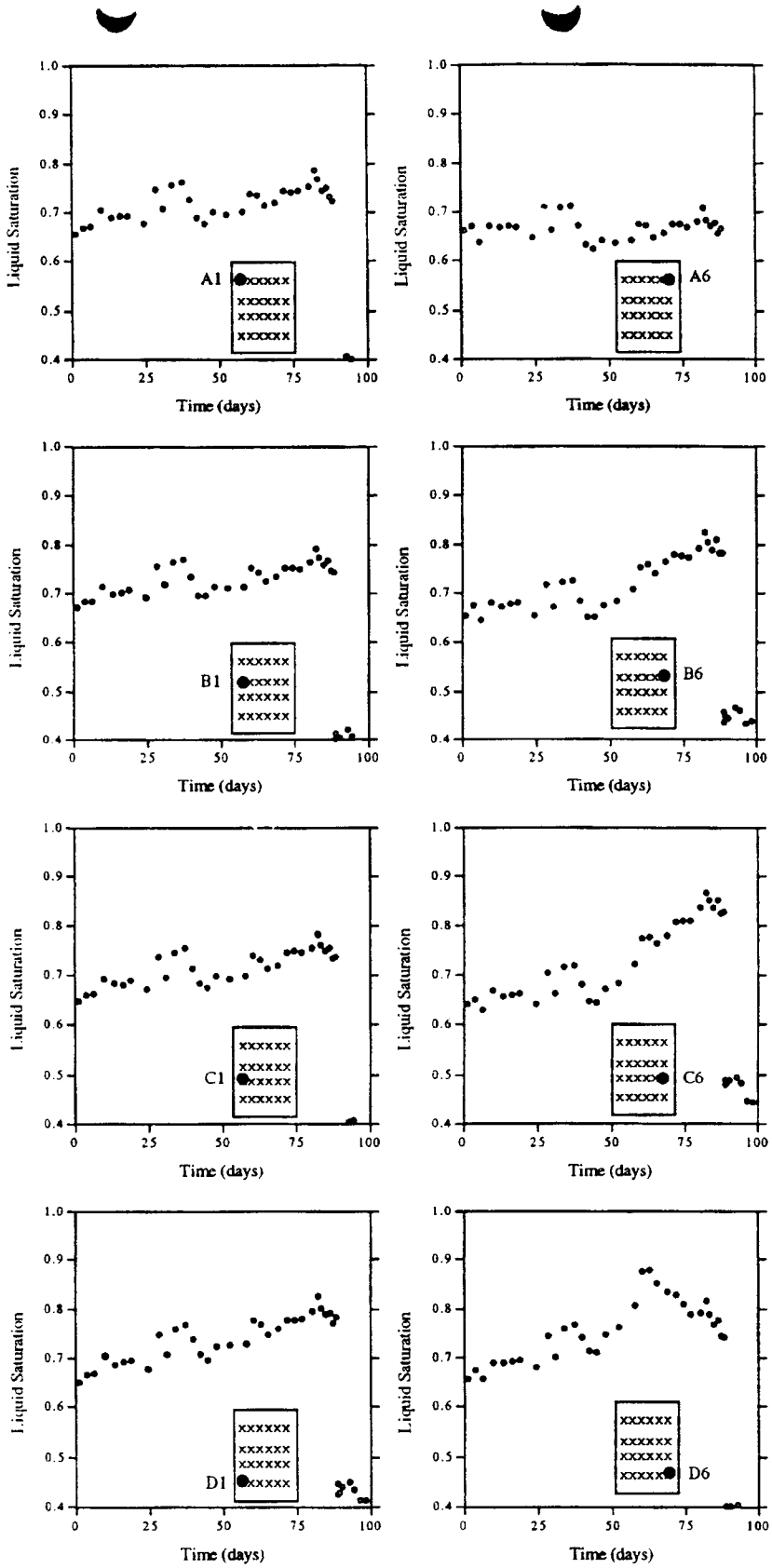

Figure 10. Liquid saturation based on gamma-ray densitometer measurements in test 1 (insets show measurement locations).

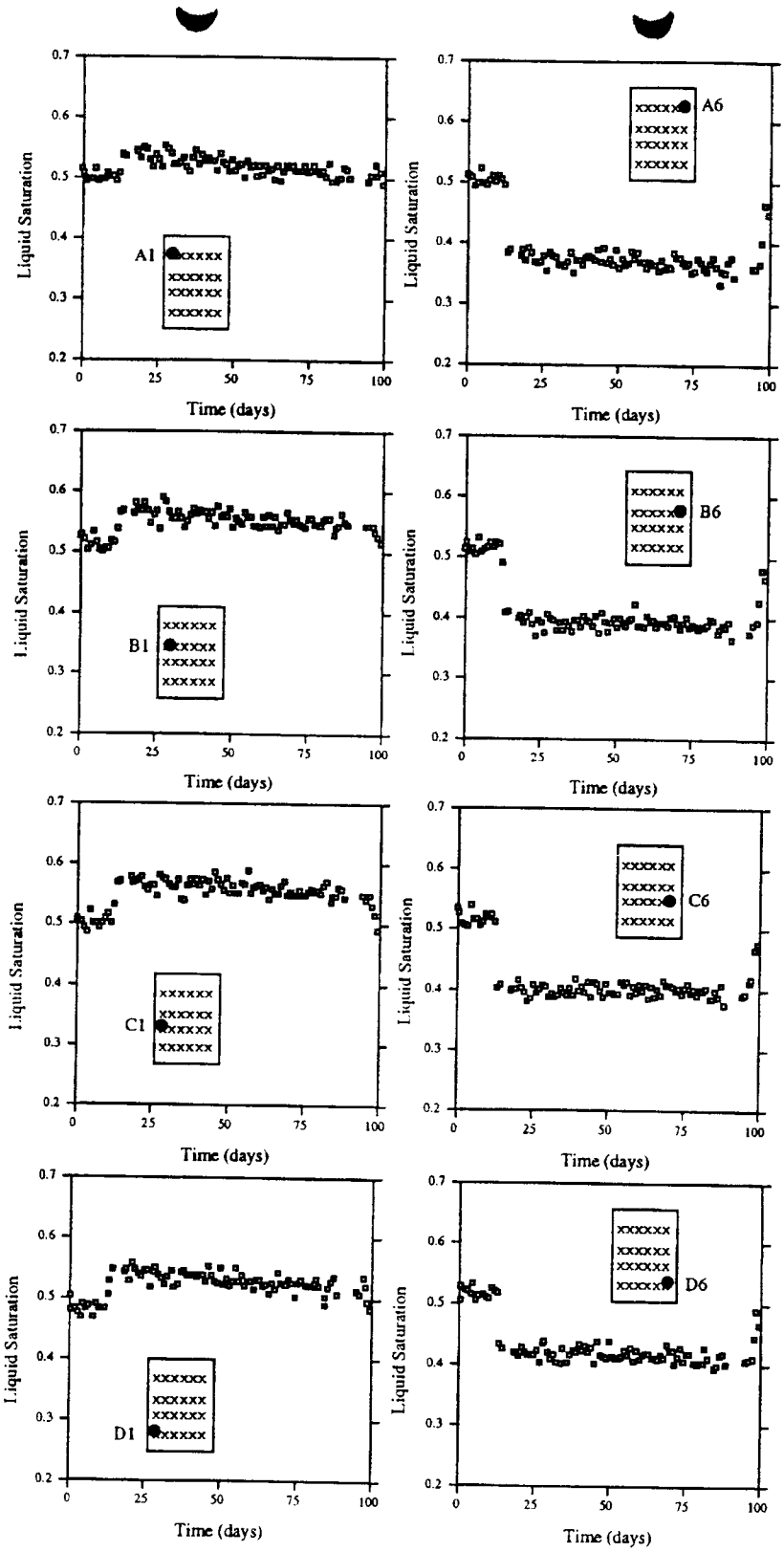

Figure 11. Liquid saturation based on gamma-ray densitometer measurements in test 2 (insets show measurement locations).

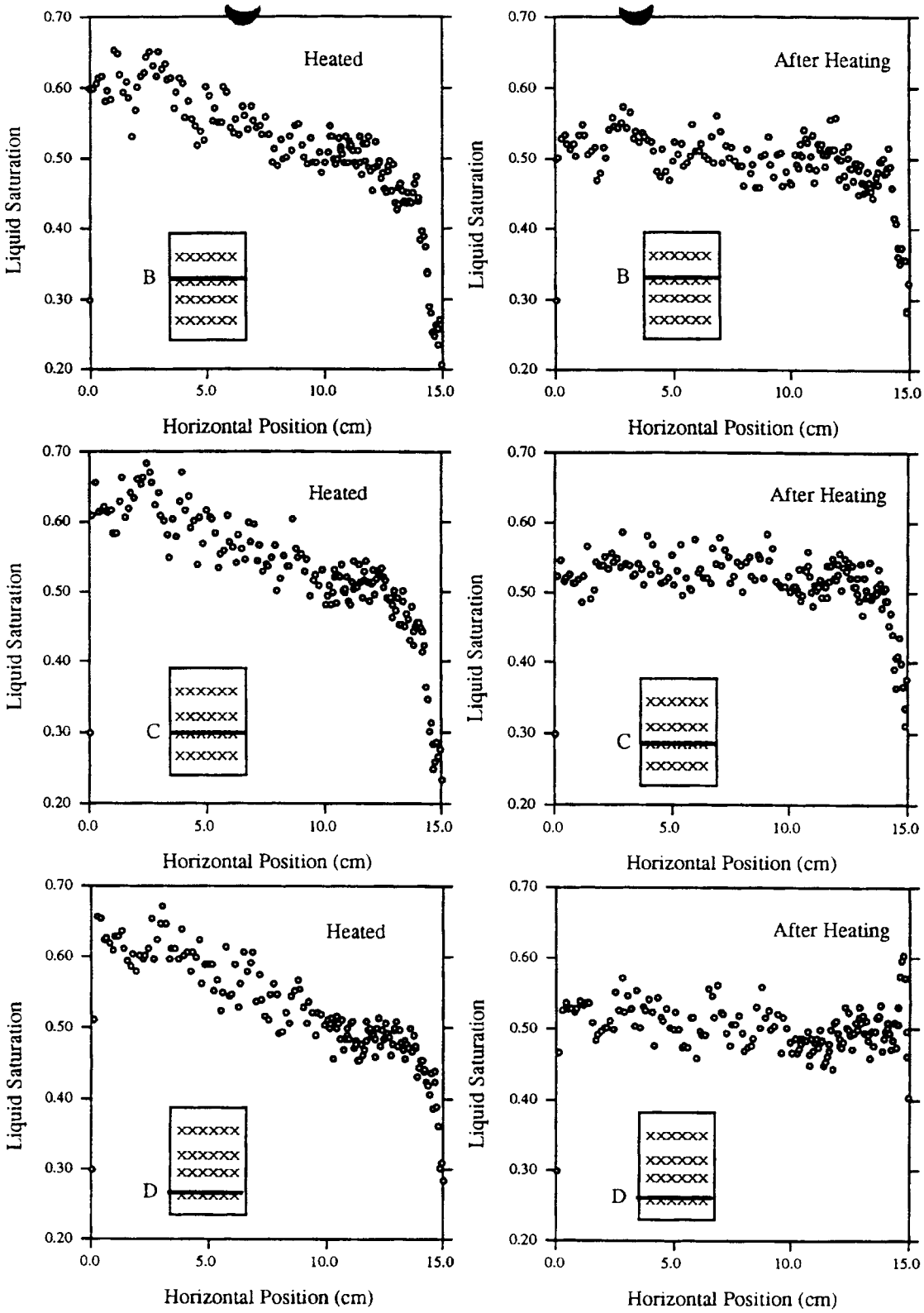

Figure 12. Horizontal liquid saturation profiles based on gamma-ray densitometer measurements in test 2 (insets show measurement locations).

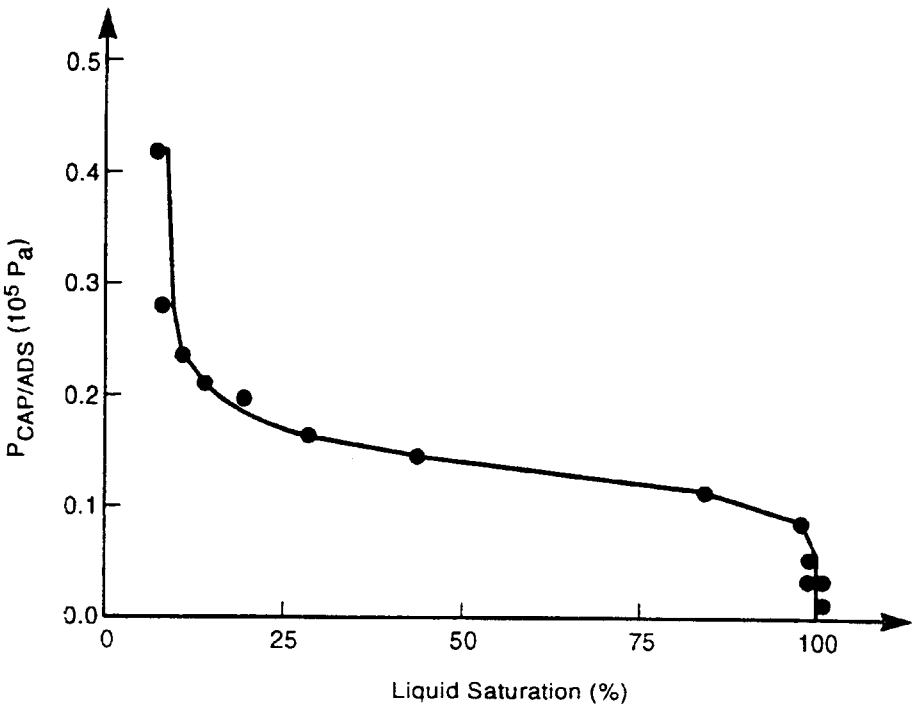

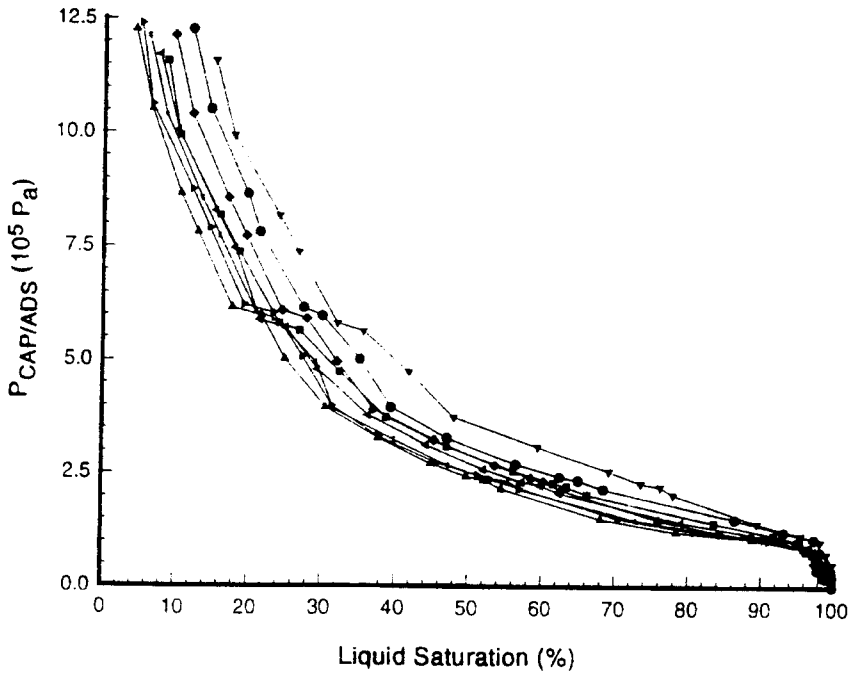

Figure 13. Characteristic curves for the porous medium used in test 1 (above) and test 2 (below).

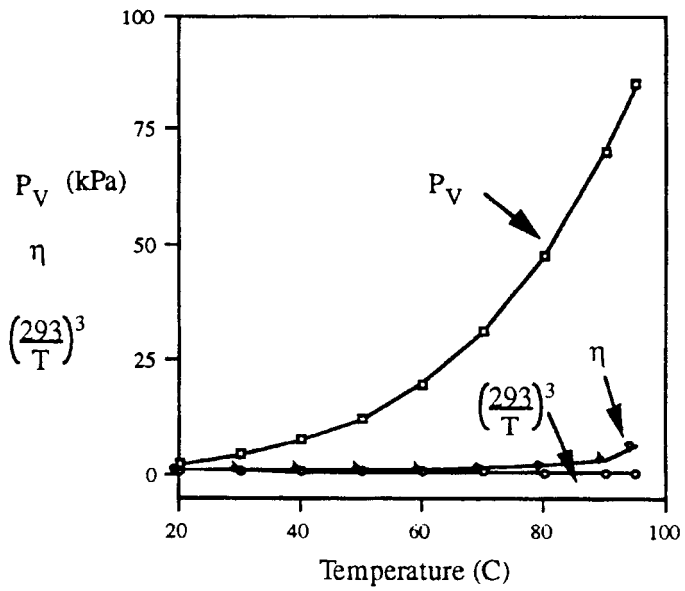

Figure 14. Comparison of the temperature dependance of P_V, η, and $(293/T)^3$.

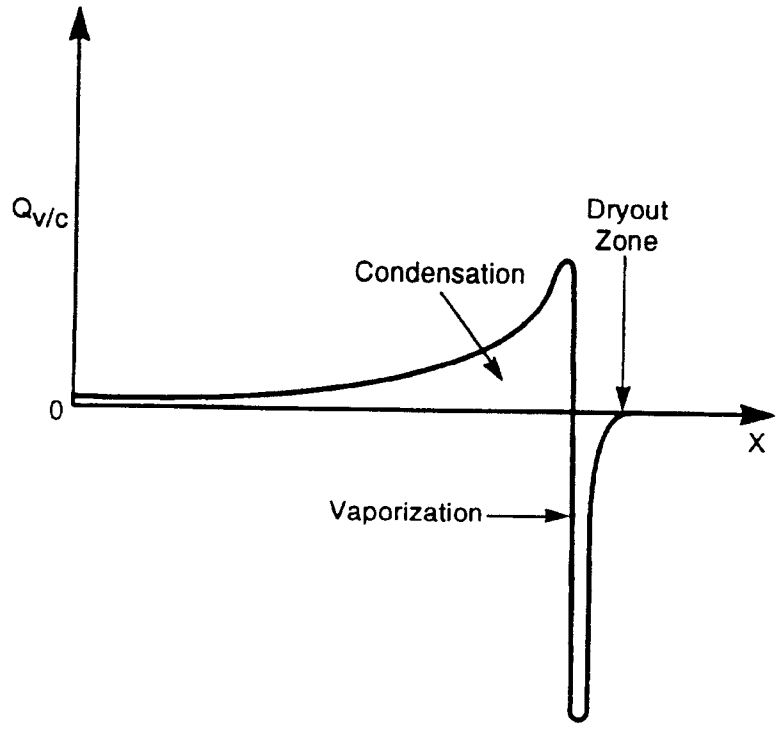

Figure 15. Illustration of $Q_{V/C}$ showing the condensation, vaporization and dryout zones.